NASA/TP-1999-209362

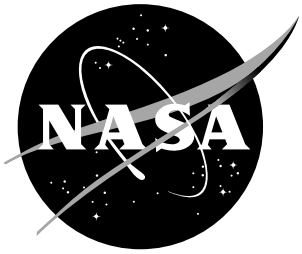

Surface Emissivity Maps for Use in Satellite Retrievals of Longwave Radiation

Anne C. Wilber
Analytical Services and Materials, Inc., Hampton, Virginia

David P. Kratz
Langley Research Center, Hampton, Virginia

Shashi K. Gupta
Analytical Services and Materials, Inc., Hampton, Virginia

August 1999

The NASA STI Program Office ... in Profile

Since its founding, NASA has been dedicated to the advancement of aeronautics and space science. The NASA Scientific and Technical Information (STI) Program Office plays a key part in helping NASA maintain this important role.

The NASA STI Program Office is operated by Langley Research Center, the lead center for NASA's scientific and technical information. The NASA STI Program Office provides access to the NASA STI Database, the largest collection of aeronautical and space science STI in the world. The Program Office is also NASA's institutional mechanism for disseminating the results of its research and development activities. These results are published by NASA in the NASA STI Report Series, which includes the following report types:

- TECHNICAL PUBLICATION. Reports of completed research or a major significant phase of research that present the results of NASA programs and include extensive data or theoretical analysis. Includes compilations of significant scientific and technical data and information deemed to be of continuing reference value. NASA counterpart of peer-reviewed formal professional papers, but having less stringent limitations on manuscript length and extent of graphic presentations.

- TECHNICAL MEMORANDUM. Scientific and technical findings that are preliminary or of specialized interest, e.g., quick release reports, working papers, and bibliographies that contain minimal annotation. Does not contain extensive analysis.

- CONTRACTOR REPORT. Scientific and technical findings by NASA-sponsored contractors and grantees.

- CONFERENCE PUBLICATION. Collected papers from scientific and technical conferences, symposia, seminars, or other meetings sponsored or co-sponsored by NASA.

- SPECIAL PUBLICATION. Scientific, technical, or historical information from NASA programs, projects, and missions, often concerned with subjects having substantial public interest.

- TECHNICAL TRANSLATION. English-language translations of foreign scientific and technical material pertinent to NASA's mission.

Specialized services that complement the STI Program Office's diverse offerings include creating custom thesauri, building customized databases, organizing and publishing research results ... even providing videos.

For more information about the NASA STI Program Office, see the following:

- Access the NASA STI Program Home Page at ***http://www.sti.nasa.gov***

- E-mail your question via the Internet to help@sti.nasa.gov

- Fax your question to the NASA STI Help Desk at (301) 621-0134

- Phone the NASA STI Help Desk at (301) 621-0390

- Write to:
  NASA STI Help Desk
  NASA Center for AeroSpace Information
  7121 Standard Drive
  Hanover, MD 21076-1320

NASA/TP-1999-209362

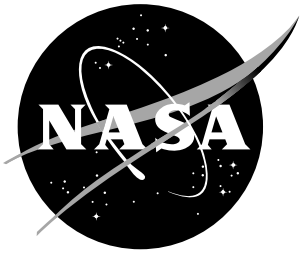

Surface Emissivity Maps for Use in Satellite Retrievals of Longwave Radiation

Anne C. Wilber
Analytical Services and Materials, Inc., Hampton, Virginia

David P. Kratz
Langley Research Center, Hampton, Virginia

Shashi K. Gupta
Analytical Services and Materials, Inc., Hampton, Virginia

National Aeronautics and
Space Administration

Langley Research Center
Hampton, Virginia 23681-2199

August 1999

Available from:

NASA Center for AeroSpace Information (CASI)
7121 Standard Drive
Hanover, MD 21076-1320
(301) 621-0390

National Technical Information Service (NTIS)
5285 Port Royal Road
Springfield, VA 22161-2171
(703) 605-6000

Abstract

An accurate accounting of the surface emissivity is important both in the retrieval of surface temperatures and in the calculation of the longwave surface energy budgets which are derived from data collected by remote sensing instruments aboard aircraft and satellites. To date, however, high quality surface emissivity data have not been readily available for global applications. As a result, many remote sensing and climate modeling efforts have assumed the surface to radiate as a blackbody (surface emissivity of unity).

Recent measurements of spectral reflectances of surface materials have clearly demonstrated that surface emissivities deviate considerably from unity, both spectrally and integrated over the broadband. Thus, assuming that a surface radiates like a blackbody can lead to potentially significant errors in surface temperature retrievals in longwave surface energy budgets and in climate studies. Taking into consideration some recent spectral reflectance measurements, we have constructed global maps of spectral and broadband emissivities that are dependent on the scene (or surface) type. To accomplish our goal of creating a surface emissivity map, we divided the Earth's surface into a 10′ lat. X 10′ lon. grid, and categorized the land surface into 18 scene types. The first 17 scene types correspond directly to those defined in the International Geosphere Biosphere Programme (IGBP) surface classification system. Scene type 18 has been added to represent a tundra-like surface which was not included in the IGBP system. Laboratory measurements of the spectral reflectances for different mineral and vegetation types were then associated, individually or in combination, with each of the 18 surface types, and used to estimate the emissivities of those surface types. Surface emissivity maps were generated from the band-averaged laboratory data for 12 longwave spectral bands (> 4.5 μm) used in a radiative transfer code as well as for the NASA's Clouds and the Earth's Radiant Energy System (CERES) window channel band (8–12 μm). The spectral emissivities for the 12 spectral bands were subsequently weighted using the Planck function energy distribution to calculate a broadband longwave (5–100 μm) emissivity. The resulting broadband emissivities were used with a surface longwave model to examine the differences resulting from the use of the emissivity maps and the blackbody assumption.

Introduction

Measuring the longwave (LW) radiation budget at the Earth's surface is a critical part of NASA's Clouds and the Earth's Radiant Energy System (CERES) project (Wielicki *et al.* 1996). Such LW measurements will foster a better understanding of the energetics of the Earth's atmosphere-surface system. Accurately characterizing surface emissivity (ε) is important for correctly determining the longwave radiation leaving the surface and for retrieving surface temperature from remote sensing measurements (Wan and Dozier 1996; Kahle and Alley 1992; Kealy and Hook 1993). Frequently, past studies have assumed the emissivity to be unity when determining surface temperature and longwave emission. To improve the accuracy of retrieved satellite products, global maps have been created of surface emissivities for 12 longwave spectral bands of the Fu-Liou radiative transfer model (Fu and Liou 1992), for the CERES window channel (8–12 μm), and for the broadband longwave region.

Ideally, field measurements of a wide range of surface types (e.g., soils, crops, forests, grasslands, and semi-arid) would be sufficient to construct surface emissivity maps. Accurate in-situ measurements of emissivity, however, are very difficult to obtain because the parameters which influence apparent emissivity, namely the surface temperature and atmospheric state, are highly variable quantities and are difficult to measure. In addition, the spatial coverage of the available field measurements is insufficient for global studies. Remote sensing measurements from satellites could be used to retrieve surface emissivities, but that requires concurrent temperature measurements on the ground as well as detailed knowledge of atmospheric absorption and scattering. With a single measurement of surface temperature or emissivity, the problem is undetermined. Many methods have been used to approach this problem. There has been some success (Van de Griend and Owe 1993; Olioso 1995) in relating the thermal emissivity to the Normalized Difference Vegetation Index (NDVI) from the Advanced Very High Resolution Radiometer (AVHRR). Several algorithms have been developed for use with the new generation of satellite instruments. The Advanced Spaceborne Thermal Emission and Reflection Radiometer (ASTER), the Moderate Resolution Imaging Spectroradiometer (MODIS), and the Process Research by Imaging Space Mission (PRISM) instruments will all use temperature-emissivity separation algorithms to retrieve surface temperature and surface emissivities from remote measurements (Caselles *et al.* 1997). The new generation of satellite instruments and the current thrust of field experiments will help to fill the gap in our knowledge of surface emissivity.

Algorithms developed for the CERES processing use surface emissivity to determine the longwave radiation budget at the Earth's surface. As a consequence, surface emissivity maps were needed as soon as the CERES instrument began taking measurements. Nevertheless, surface emissivities from other EOS instruments will not be made available until 3 to 5 years after the launch of the first CERES instrument. We have, therefore, created surface emissivity maps from laboratory measurements. Such maps will constitute a viable source for surface emissivity data until the EOS surface emissivity measurements become available to create more advanced maps.

The emissivity of the ocean surface is known to vary with the viewing zenith angle and the sea state. When determining the sea surface temperature from space, this variation is important. The effects of viewing angle and sea state on emissivity have been both modeled and

measured (Masuda *et al*. 1988; Smith *et al*. 1996; Wu and Smith 1997); however, it has been found that at near-nadir viewing angles both spectral and broadband surface emissivities are nearly constant with respect to sea state. Since the present global emissivity maps have been developed for nadir viewing conditions, we do not need to consider the effect of sea state on emissivity. More advanced versions of the surface emissivity map will consider sea state whenever zenith angle effects are included.

To accomplish the goals of the CERES project, the Surface and Atmospheric Radiation Budget (SARB) group in the CERES experiment created a global scene type map on a 10′ grid (Rutan and Charlock 1997). The scene types for this map were adopted from the International Geosphere Biosphere Programme (IGBP) classification for the Earth's surface with an additional scene type for tundra. Global maps of broadband and spectral albedos necessary for calculating the shortwave (SW) portion of the radiation budget were developed based on the IGBP scene types. The present emissivity maps have, for the sake of consistency, utilized the same IGBP scene types and thus are compatible with the albedo maps. The MODIS instrument team has also proposed using a classification-based method to determine surface emissivity (Snyder *et al*. 1998). For instance, the MODIS team will use surface emissivity data for MODIS channels 31 and 32 in order to retrieve land surface temperature. Laboratory measurements of the spectral reflectances of several different vegetation and soil types found in the Johns Hopkins Spectral Library (Salisbury and D'Aria 1992a) have been used to compute spectral emissivities for each of the 18 surface types. The spectral reflectance data have been used to calculate band-average emissivity in each of the 12 spectral bands used in the Fu-Liou radiative transfer model. The 12 band-average emissivities were combined into broadband emissivity by weighting with the Planck function energy distribution. The CERES window channel has also been subdivided into three bands. The emissivities of the three bands were then combined into a window emissivity in the same manner as the broadband.

The global emissivity maps presented herein are the first to handle surface emissivity on a scene dependent basis. Until surface emissivity measurements become available for a representative fraction of the earth, it is beneficial to have global maps of surface emissivity based on surface type using presently available measurements. The global surface emissivity maps will be modified as more laboratory and field data become available. In addition, data received from the MODIS and ASTER instruments will also be incorporated. Even after we make available more advanced versions of the emissivity maps which consider zenith angle effects, seasonal effects, and wider variety of surface types, the present emissivity map should still prove useful for use by models where more complex maps are not warranted.

Theory and Background

Laboratory measurements have been made for the spectral reflectances of a wide variety of surface materials (Salisbury and D'Aria 1992a). Since the CERES processing algorithms require surface emissivities, the measured reflectances were transformed into emissivities by applying energy conservation and Kirchhoff's Law.

For a process involving absorption, reflection, and transmission, the total energy, normalized to unity, is partitioned as:

$$A_\lambda + R_\lambda + T_\lambda = 1. \quad (1)$$

The present study assumes the transmittance (T_λ) of the surface to be zero. Applying Kirchhoff's Law which states that the absorptance (A_λ) is equal to the emittance (ε_λ) under conditions of thermodynamic equilibrium yields a straightforward relationship between reflectance (R_λ.) and emissivity:

$$\varepsilon_\lambda = 1 - R_\lambda. \quad (2)$$

Figure 1 shows emissivity as a function of wavelength derived from laboratory measurements for nine materials representative of a large percentage of the Earth's surface.

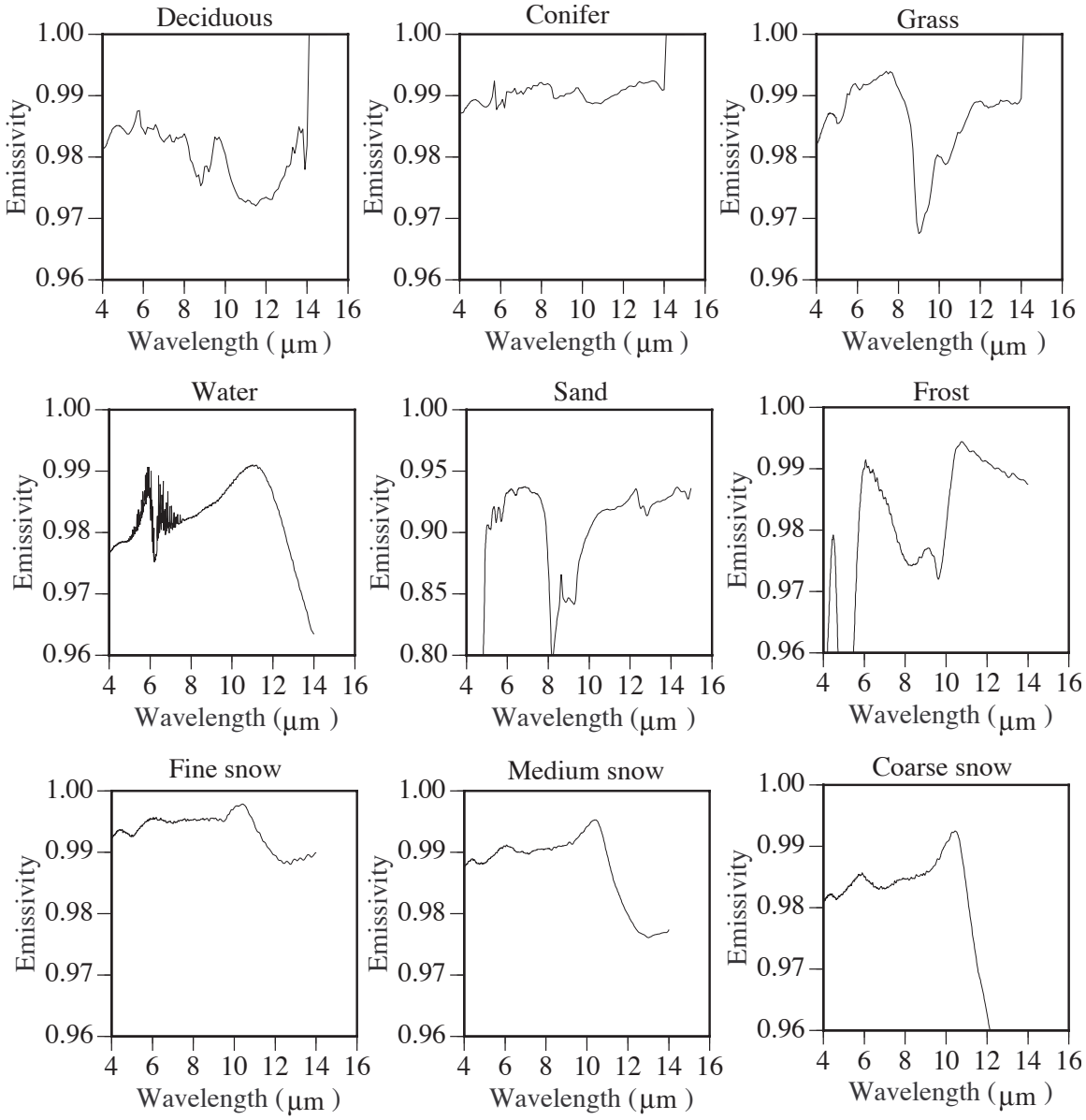

Figure 1. Emissivity from Laboratory Measurements for 9 Materials.

Fu and Liou (1992) developed the radiative transfer code which is being used by the SARB group in the CERES experiment. The code uses a delta-four-stream (Liou *et al.* 1988) approach for scattering and a set of correlated k-distributions for absorption in 18 distinct spectral bands. This code divides the shortwave region (0.2–4.5 μm) into six bands, and the longwave (> 4.5 μm) into 12 bands. The longwave bands, which cover the spectral range of interest in this report, are presented in Table 1.

Table 1. Specification of Fu-Liou bands in the longwave region.

Band	Wavelength (μm)	Wavenumber (cm^{-1})
1	4.5–5.3	2200–1900
2	5.3–5.9	1900–1700
3	5.9–7.1	1700–1400
4	7.1–8.0	1400–1250
5	8.0–9.1	1250–1100
6	9.1–10.2	1100–980
7	10.2–12.5	980–800
8	12.5–14.9	800–670
9	14.9–18.5	670–540
10	18.5–25.0	540–400
11	25.0–35.7	400–280
12	>35.7	280–0

The choice of wavelength ranges for the bands in a radiative transfer model is based primarily on the absorption/emission characteristics of the atmospheric constituents. However, radiative characteristics of the surface in these bands are just as important for analyzing the radiation measurements. A brief description of the absorption/emission processes in each of the Fu- Liou bands, and the resulting relationship betwen emissivity and outgoing LW radiation are presented below.

Fu-Liou Bands

The first band (4.5–5.3 μm) is fairly transparent; however, the energy emitted from the surface in this spectral range is quite small. As a result, this spectral range does not provide a great deal of information concerning surface and lower tropospheric properties. Bands 2 and 3 (5.3–5.9 μm and 5.9–7.1 μm) encompass the very strong 6.3 μm band of water vapor. Thus, very little energy emitted from the surface is transmitted through the atmosphere in this wavelength range. Band 4 (7.1–8.0 μm) involves the important absorption due to the minor trace gases CH_4 and N_2O, as well as additional water vapor absorption. The CH_4 absorption band centered at 7.7 μm, and the N_2O absorption band centered at 7.8 μm are important contributors to the atmospheric greenhouse effect. Since the 7.1–8.0 μm spectral range allows some emitted surface radiation to escape to space, the surface emissivity becomes important to TOA measurements in this spectral range. When taken together, bands 5, 6 and 7 (8.0–9.1 μm, 9.1–10.2 μm, and 10.2–12.5 μm) correspond very closely to the CERES window channel. Since the rationale behind subdividing this spectral range is valid both for running the Fu-Liou model and for processing the CERES measurements, these intervals will be discussed in detail when we discuss the CERES window channel. Note, the spectral regions are by far the most transparent in the infrared. Thus, outgoing radiances in these regions coressponding to the CERES window channel are strongly affected by the surface emissivity. Bands 8 and 9 (12.5–14.9 μm and 14.9–18.5 μm) are characterized by the very strong 15 μm band of CO_2. While there is also a small amount of water vapor absorption within

these spectral intervals, it is the CO_2 absorption which dictates the widths of these spectral bands. Absorption and emission due to CO_2 in the 15 μm band provides an important source of radiative cooling throughout the atmosphere. The spectral interval from 12.5–14.9 μm allows some radiation to escape to space, most notably near the short wavelength end. The spectral interval from 14.9–18.5 μm is essentially opaque to surface emission. Bands 10, 11 and 12 (>18.5 μm) represent the water vapor pure rotation band. Because the pure rotation band of water vapor covers a rather wide spectral range and the absorption is far from uniform in nature, this spectral range has been subdivided into the three intervals. For conditions where water vapor burden is very low (< 3 kg m^{-2}), the 18.5–25.0 μm band becomes relatively transparent, and is sometimes referred to as the "dirty window" or the "polar window" band. Thus, surface emissivity may be important in the 18.5–25.0 μm band.

CERES Window channel

The CERES window channel measures the thermal infrared energy emitted from the Earth within the spectral range between 8 and 12 μm. The CERES window channel is nearly ideal for measuring the energy emanating from the proximity of the Earth's surface because its wavelength range corresponds to the most transparent part of the infrared spectrum. These measurements provide valuable information concerning atmosphere-surface interactions. Recent measurements (Salisbury and D'Aria 1992a) have demonstrated that the emissivities of typical terrestrial materials (soils, vegetation, water, etc.) can be significantly less than unity and are quite variable over the spectral range of the CERES window channel. Moreover, while the window region is relatively transparent, within this spectral range there exists a significant amount of highly nonuniform molecular absorption due to H_2O and O_3, as well as a host of minor trace species (Kratz and Rose 1999). Furthermore, the opacity of thin cirrus clouds tends to increase significantly toward both longer and shorter wavelengths within this spectral range (see e.g., Figure 2 of Prabhakara *et al.* 1993). The distribution of these processes within the CERES window channel has prompted the subdivision of the CERES window channel into three distinct subintervals, as shown in Table 2. Data from these 3 spectral intervals will ensure accurate modeling of top-of-atmosphere (TOA) radiation in the CERES window channel.

Table 2. Specification of the sub-intervals of the CERES window channel.

Band	Wavelength (μm)	Wavenumber (cm^{-1})
1	8.0–9.1	1250–1100
2	9.1–10.2	1100–980
3	10.2–12.0	980–835

The subinterval covering the 8.0–9.1 μm range is associated with the very strong asymmetric stretching fundamental bands (reststrahlen bands) of quartz. Within this subinterval, bare soils have characteristically low emissivities. In contrast, the highest emissivities for senescent leaves occur within the 8.0–9.1 μm spectral range. Moderately weak absorption due to H_2O, as well as minor absorption due to O_3, N_2O, and CH_4 also occur within the 8.0–9.1 μm spectral range. In addition, thin cirrus clouds possess a relatively high opacity in this subinterval. For the subinterval covering the 9.1–10.2 μm range, upwelling TOA flux is strongly affected by the 9.6 μm band of O_3. The presence of this strong O_3 band along with some additional absorption due to H_2O and CO_2 prevents direct sensing of the surface by

satellites within the 9.1–10.2 μm range. Thin cirrus clouds possess a somewhat lower opacity in this subinterval as compared with the other two CERES window channel subintervals. The last subinterval, (10.2–12.0 μm), has surface emissivities for bare soils that tend to be relatively high. In addition, the highest emissivities for green foliage occur within this spectral range. The moderately weak H_2O absorption, as well as the smaller, yet significant contribution from the 10.4 μm band of CO_2 also affect this interval. The opacity of the cirrus clouds in this subinterval is comparable to that of the first subinterval.

Method of Band Averaging and Weighting

The emitted spectral radiance L_λ at wavelength λ from a surface at temperature T_s is calculated by multiplying the Planck function, $B_\lambda(T_s)$ by the spectral emissivity ε_λ

$$L_\lambda(T_s) = \varepsilon_\lambda B_\lambda(T_s). \tag{3}$$

The Planck function, $B_\lambda(T_s)$ represents the radiance emitted by a blackbody at a wavelength λ and a surface temperature T_s.

Integrated over all wavelengths:

$$\pi \int_0^\infty B_\lambda(T_s)\, d\lambda = \sigma T_s^4 \ , \tag{4}$$

where σ is the Stephen-Boltzman Constant (5.67×10^{-8} W m^{-2}K^{-4}).

The band-average emissivity in band i, from Tables 1 or 2, is defined by:

$$\bar{\varepsilon}_i = \frac{\int_{\lambda_{(i,lower)}}^{\lambda_{(i,upper)}} \varepsilon_\lambda B_\lambda(T) d\lambda}{\int_{\lambda_{(i,lower)}}^{\lambda_{(i,upper)}} B_\lambda(T) d\lambda} \tag{5}$$

The Planck function term in equation (5) can be taken out of the weighting process without introducing significant error. Such a strategy can be used for the following reasons. First, the wavelength dependence of the Planck function is relatively weak for the small intervals considered by Table 1. Second, the temperature dependence of the emissivity is usually very small for most surface materials. Even for coarse sands, which show the most variation, the band-averaged emissivity in the 3.5–4.25 μm band changes only 0.004 as the temperature changes from 240 to 320 K (Wan and Dozier 1996). Third, the spectral dependence of the surface emissivity is not generally correlated with the spectral dependence of the Planck function. Thus, the band emissivity calculated from laboratory reflectance spectra of a pure material becomes

$$\bar{\varepsilon}_i = \frac{\int_{\lambda_{(i,\,lower)}}^{\lambda_{(i,\,upper)}} \varepsilon_\lambda \, d\lambda}{\int_{\lambda_{(i,\,lower)}}^{\lambda_{(i,\,upper)}} d\lambda}, \tag{6}$$

which is taken to be independent of surface temperature because, as noted previously, the temperature dependence is usually very small. Equation (6) is used to calculate band-averaged emissivity. Figure 2 shows the location of the Fu-Liou spectral bands relative to the laboratory measured emissivity of a conifer sample.

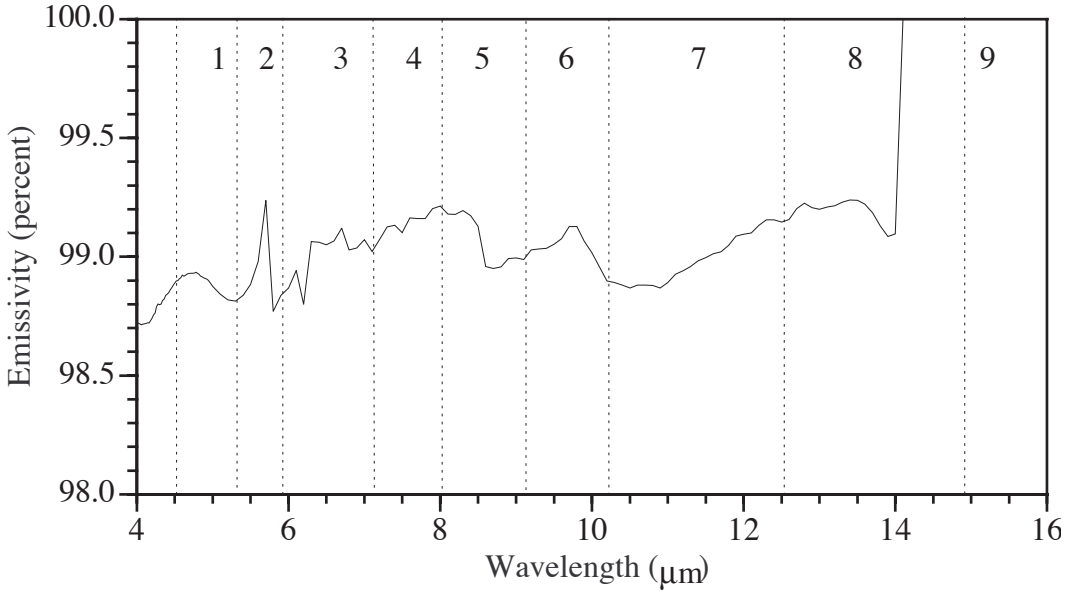

Figure 2. Locations of Fu-Liou Bands from Table 1 Relative to Laboratory Measurements of Conifer Sample.

In general, the laboratory measurements spanned the wavelength range of 2–16 μm. At wavelengths greater than 16 μm, the emissivity was extrapolated, i.e., the measured emissivity in the interval closest to 16 μm was replicated to fill the remaining bands where data were not available.

Using equation (6), we calculated 12 band-averaged emissivities for the Fu-Liou bands and 3 band-averaged values for the CERES window channel. To calculate a broadband emissivity from the band-average emissivities, the Planck function was used to energy weight each of the 12 band-average emissivities. The weighted values were then combined into a broadband emissivity. A weighting factor (*wf*) was calculated for each of the 12 bands as

$$wf_i = \frac{\int_{\omega_{(i,lower)}}^{\omega_{(i,upper)}} B_\omega d\omega}{\int_0^{2200} B_\omega d\omega}, \quad (7)$$

where, $B_\omega d\omega = B_\lambda d\lambda$, wf_i is the weighting factor for a band and $\omega_{i,upper}$ and $\omega_{i,lower}$ are the upper and lower wavenumbers for each spectral band from Table 1. It is more convenient to use wavenumber space in the infrared to integrate over small intervals of the order of 10 cm^{-1}. Therefore, the Planck function was expressed in terms of wavenumber and integrated. The conversion factor from wavelength (μm) to wavenumber (cm^{-1}) is: $\omega(cm^{-1})=10000/\lambda$ (μm) [e.g., 1 μm = 10000 cm^{-1}]. In this manner a weighting factor was calculated for each band. The broadband emissivity, ε_{bb} was then calculated by

$$\varepsilon_{bb} = \sum_{i=1}^{i=12} wf_i \varepsilon_i . \quad (8)$$

Differences in temperature had no significant effect in the broadband calculation except for some minor effect in the case of quartz sand; therefore, a temperature of 288 K, which is representative of the average surface temperature of the Earth, was chosen for the calculation of the weighting factors. Note that a variation in temperature from 263 to 313 K resulted in a change of 0.011 in broadband emissivity for quartz. The change in emissivity of vegetation was 0.002 for the same variation in temperature. The weighting factors described in equation (7) were also used to combine the emissivities of the sub-intervals of the CERES window channel emissivity.

Data

Until recently, no emissivity data for vegetation were available in the thermal infrared region. Because of improvements in detector technology and measurement methods, measurements of spectral reflectivity have become available for various land cover types. We used the data from the Johns Hopkins Spectral Library. The ASTER team is also using this spectral library and has created an easily accessible database located at:

http://speclib.jpl.nasa.gov/

Data consist of laboratory measurements of reflectance of various types of vegetation, soils and snow and ice.

Information on the measurement techniques is available at:

http://speclib.jpl.nasa.gov/documents/jhu_desc.htm

http://speclib.jpl.nasa.gov/archive/JHU/becknic/vegetation/vegetation.txt

http://speclib.jpl.nasa.gov/archive/JHU/becknic/water/snow&ice.txt

All spectra in the Johns Hopkins Spectral Library were measured under the direction of John W. Salisbury. Two similar instruments were used to record reflectance in the infrared range between 2.08–15 μm. Both are Nicolet FTIR spectrophotometers and both have a reproducibility and absolute accuracy better than plus or minus 1 percent over most of the spectral range. The data were quality checked at Johns Hopkins University (JHU). The instruments record spectral data in wavenumber space where both wavenumber accuracy and spectral resolution are given in wavenumbers (cm^{-1}). Wavenumber accuracy was limited by the spectral resolution, which yields a data point every 2 wavenumbers (cm^{-1}) for these measurements. The x-axis was changed from wavenumbers (cm^{-1}) to wavelength (μm) for all of the data before use in the present calculations.

Spectra of vegetative canopy are not readily measurable. The lack of availability of field spectrometers and the effect of atmospheric absorption create difficulties in making field measurements. These problems are being overcome (Snyder and Wan 1996) and the results from the relevant studies will be included in future releases of the emissivity maps. Laboratory measurements have been made of simulated canopies from which the present data were derived.

Measurement of the spectra of many different types of vegetation showed that conifer needles, deciduous tree leaves, and grass blades all have a very low reflectance (high emissivity) throughout the thermal infrared range. Because of the low reflectance and small spectral variation, one typical deciduous leaf spectrum was chosen to represent all deciduous species, one conifer to represent all conifers, and one grass species to represent all grasses. In a canopy, Salisbury and D'Aria (1992a) have noted several factors which combine to result in an emissivity quite close to unity.

Assignment of surface types

The surface types used are those from the IGBP from Belward and Loveland (1996) with the addition of tundra as type 18. Table 3 presents the 18 surface types.

Table 3. International Geosphere Biosphere Programme Global Land Cover types.

Type ID	IGBP Type
1	Evergreen Needleleaf Forest
2	Evergreen Broadleaf Forest
3	Deciduous Needleleaf Forest
4	Deciduous Broadleaf Forest
5	Mixed Forest
6	Closed Shrublands
7	Open Shrubland
8	Woody Savannas
9	Savannas
10	Grasslands
11	Permanent Wetlands
12	Croplands
13	Urban
14	Cropland/Mosaic
15	Snow and Ice
16	Barren
17	Water Bodies
18	Tundra

A more complete description of the 18 surface types is presented in Appendix A, which has been adopted from Table 1 in Belward and Loveland (1996).

Figure 3 illustrates the global distribution of the 18 surface types given by Table 3. The data is presented on the 10′ grid used by CERES.

As noted previously, the JHU spectral library contains reflectance measurements of a variety of surface materials. For the purposes of this study, 10 surface materials, individually or in combination are taken to be representative of the 18 surface types. The 10 surface materials used from the spectral library are: grass, conifer, deciduous, fine snow, medium snow, coarse snow, frost, ice, seawater, and quartz sand. The emissivity spectra of nine types of surface cover are shown in Figure 1. Table 4 shows how the 10 surface materials are associated with the 18 surface types.

Table 4. Assignment of laboratory measurements to surface types.

Type ID	IGBP type	Spectral library
1	Evergreen Needleleaf Forest	Conifer
2	Evergreen Broadleaf Forest	Conifer
3	Deciduous Needleleaf Forest	Deciduous
4	Deciduous Broadleaf Forest	Deciduous
5	Mixed Forest	1/2 Conifer + 1/2 Deciduous
6	Closed Shrublands	1/4 Quartz sand + 3/8 Conifer + 3/8 Deciduous
7	Open Shrubland	3/4 Quartz sand + 1/8 Conifer + 1/8 Deciduous
8	Woody Savannas	Grass
9	Savannas	Grass
10	Grasslands	Grass
11	Permanent Wetlands	1/2 Grass + 1/2 Seawater
12	Croplands	Grass
13	Urban	Black Body
14	Cropland/Mosaic	1/2 Grass + 1/4 Conifer + 1/4 Deciduous
15	Snow and Ice	Mean Of Fine, Medium, and Coarse snow and Ice
16	Barren	Quartz sand
17	Water Bodies	Seawater
18	Tundra	Frost

The decisions on how to associate the surface types were based on the information available, and on the authors' best judgment of how to best characterize the surface type. The evergreen needleleaf and the evergreen broadleaf were both assigned the emissivities of the conifer sample because no other evergreens were in the archive. The emissivity of the deciduous leaf was used for both the deciduous needleleaf and deciduous broadleaf. When measurements of other types of trees are available, these emissivity assignments may change, although the measurements currently available show that there is little difference between the emissivities of evergreen and deciduous forests. Because there is a lack of information on the urban surface, a blackbody emissivity of unity was assumed for all spectral regions for the urban surface type. The variations in emissivities of dry bare soil is greatest of all surface

Figure 3. Surface Types on 10' grid.

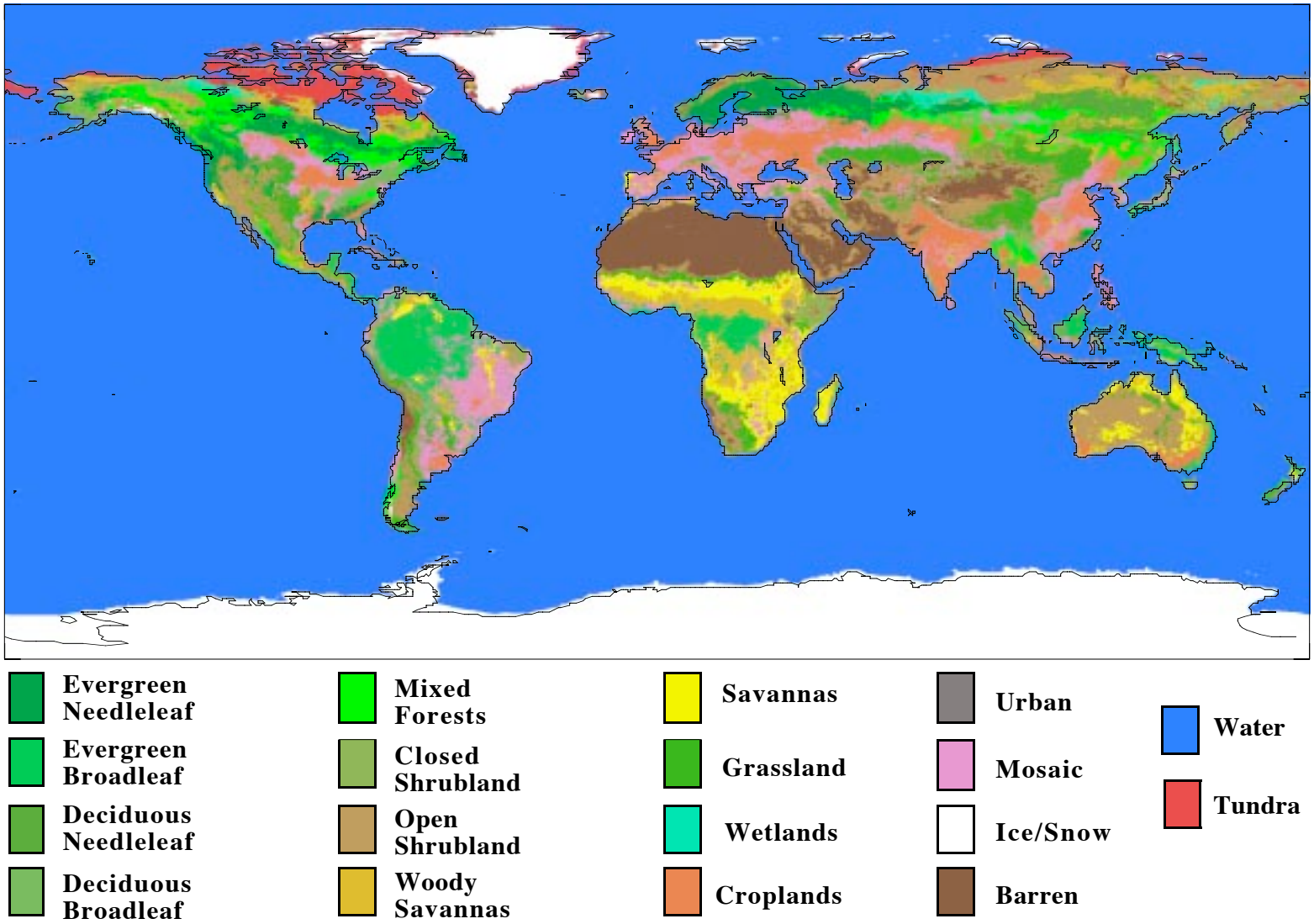

materials and therefore the most difficult to characterize. We were constrained in this version of the emissivity maps to use one emissivity classification for all the surface classified as barren. Therefore, the barren land was assigned the emissivities of a desert sample composed of mostly quartz sand. There have been few measurements made of emissivity of tundra. Though Rees (1993) has measured the thermal infrared (8-14 μm) emissivity of a number of land cover types in the Svalbard archipelago north of Norway. The observed emissivity values fell between 0.941 for sandstone and 0.995 for snow. The window emissivity of frost at 0.9806 lies within this range. Thus, the tundra surface type was assigned the emissivity of frost. When more is known about the composition and condition of tundra, the emissivity can be refined. Surface type 15 is snow and/or ice. To assign emissivity to this surface type the emissivities of the 3 snow types were averaged to create an "average snow" emissivity and then that emissivity was averaged with the emissivity of ice to create the ice/snow emissivity. Because the emissivity of ice is very close to 1, the resulting ice/snow emissivity is also close to 1.

The values of emissivity for the 12 Fu-Liou bands, the CERES window and the broadband are shown in the Table in Appendix B. Figure 4 shows the band-average emissivities of the 18 surface types. Figure 5 is the global map of broadband emissivity on the 10′ grid. Figure 6 is the global map of the CERES window channel emissivity on the 10′ grid. As additional measurements of reflectance and emittance become available, the surface emissivity maps will be updated.

Figure 4. Band-averaged Emissivities for the 18 Surface Types.

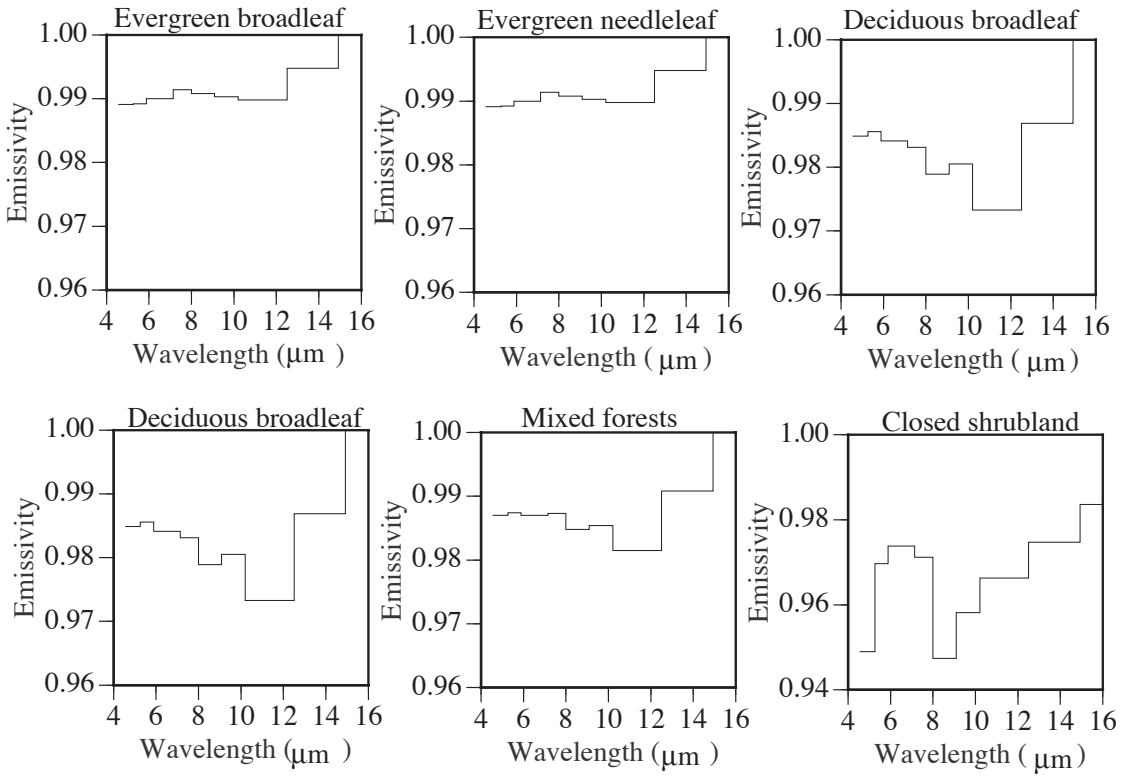

Figure 4 concluded

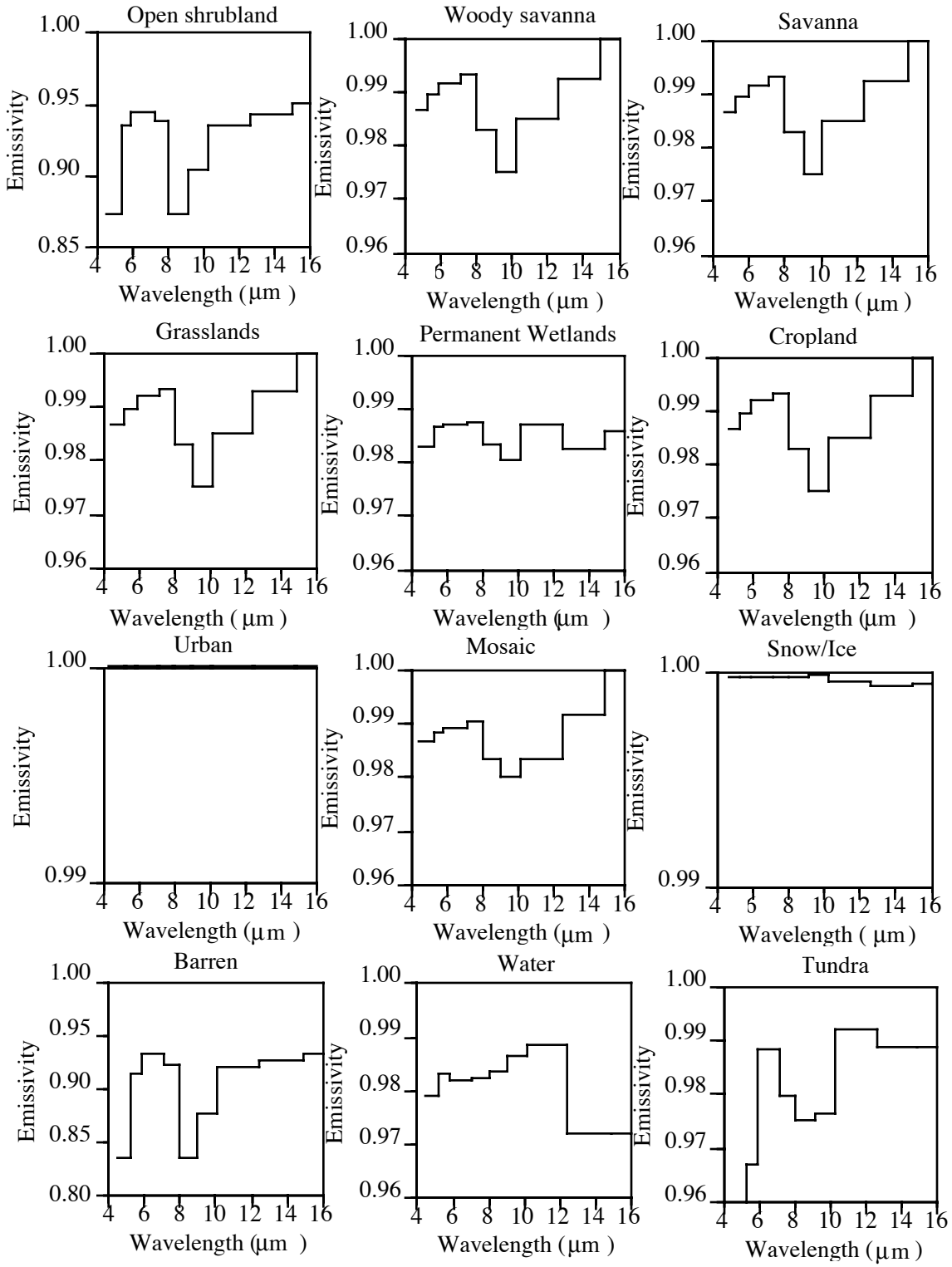

Figure 5. Broadband Surface Emissivity on 10' grid

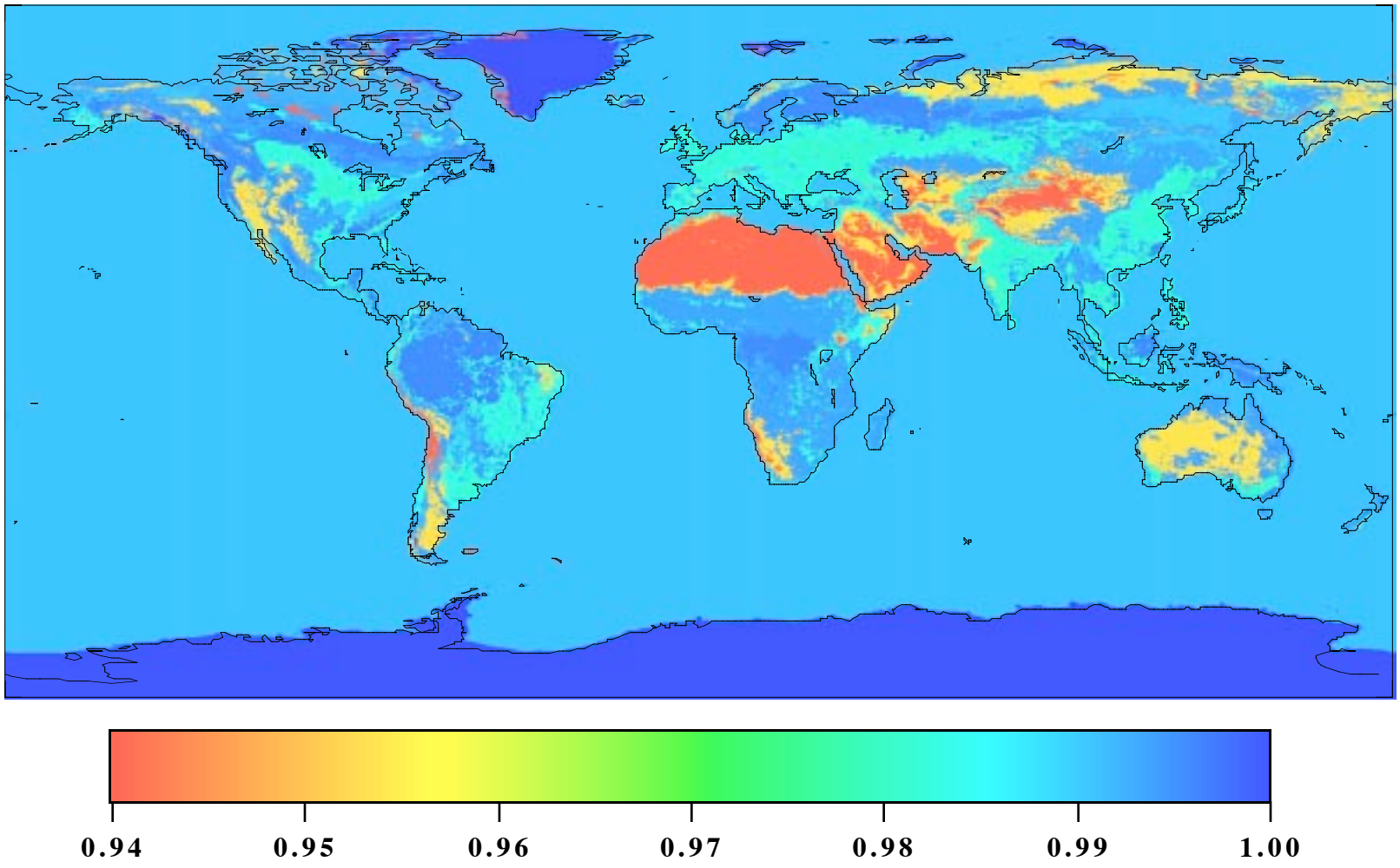

Figure 6. CERES Window (8-12 μm) Surface Emissivity on 10' grid

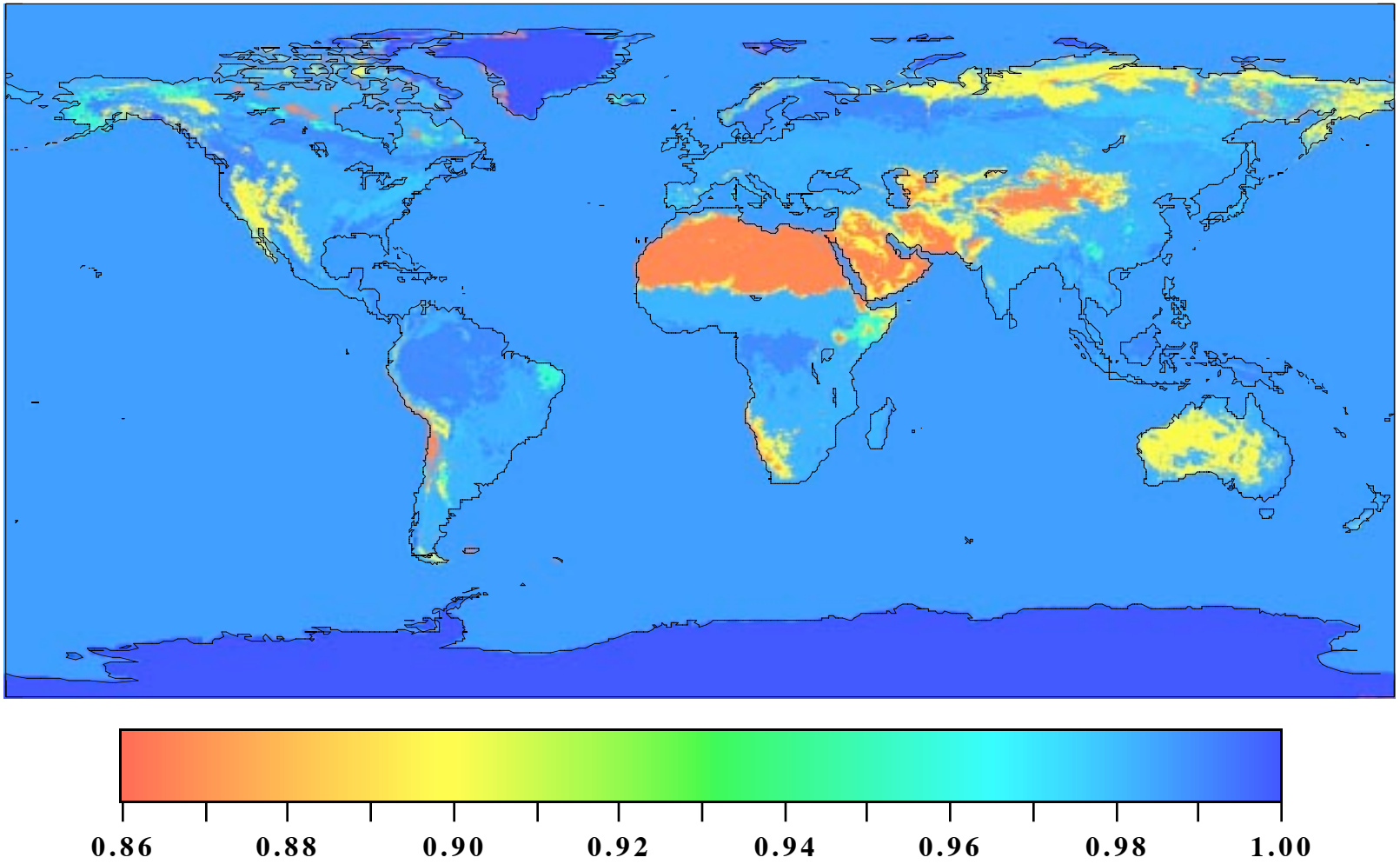

Computations using emissivity map

The effect of using the current emissivity maps on surface net longwave fluxes was examined using the Gupta longwave model (Gupta *et al.* 1992). This model is based on a parameterized radiative transfer algorithm which computes downward and net LW fluxes at the surface and has been extensively validated. This model is being used by CERES for computing surface LW fluxes. The model uses meteorology to calculate downward flux. Upward flux from the surface is calculated as $\varepsilon\sigma T^4$. The meteorological inputs for the present computation were taken from ISCCP-D1 data available on a 2.5° equal-area grid. To run the model it was first necessary to change the resolution of the broadband emissivity map, shown in Figure 5, from the 10′ to a 2.5° equal-area grid. The emissivities from the 10′ grid were averaged into a 2.5° equal-area grid. The resulting broadband emissivity map is shown in Figure 7. The model was then run assuming a constant surface emissivity of unity and again with the surface emissivity map derived in this work. The resulting net longwave fluxes are shown in Figure 8, and the difference in net longwave flux between the two different runs is shown in Figure 9. The largest differences (up to 6 Wm^{-2}) occur over areas of the Sahara Desert and the Arabian Peninsula classified as barren, and open shrubland in Australia. Differences of greater than 3 Wm^{-2} are found over the open shrubland areas of the Western US and Eurasia. There are differences of more than 1.5 Wm^{-2} over the barren areas of Siberia. Because this version of the emissivity maps was constrained to have emissivities based only on surface type, the emissivity assigned to barren ground was that of quartz sand which is appropriate for the equatorial and mid-latitude deserts but may not be applicable to the barren ground in Siberia. This treatment of barren ground will be modified as more information becomes available.

This study has shown that changing the broadband surface emissivity from a constant of unity to a variable dependent on surface type can result in differences up to 6 Wm^{-2} in the surface net longwave flux. Further refinements and improvements to the emissivity maps are necessary to account for the difference in emissivities of barren ground of the quartz deserts and the barren ground in high latitudes.

Future work

Sand and soil are the surfaces for which it is most difficult to estimate surface emissivities. They are also the surfaces for which the emissivities differ most from unity. There is large variability in emissivity dependent on composition and surface properties. Emissivity is dependent on particle size and soil moisture (Salisbury and D'Aria 1992b). In the case of sand there is also a change in emissivity with viewing angle (Snyder *et al.* 1997). All of the aforementioned influences on soil emissivity should be taken into account. The first step in improving soil emissivity estimation is to allow for more types of bare soil. The current emissivity map assumes quartz sand for the barren surface type because the largest areas of barren ground are quartz sand. Plans for modification of the emissivity map are to use the Zobler World Soil map (Zobler 1986) in conjunction with the IGBP surface type map. Currently there are no laboratory measurments made at wavelengths greater than 16 μm. It is desirable to have such measurements in the 18.5–25.0 μm for use with the "polar window" band.

The current emissivity maps are considered to be the basis upon which more refined and improved maps will be constructed as information becomes available. When emissivity

measurements from MODIS and ASTER are available, they will be incorporated into the emissivity maps. Other refinements such as incorporating seasonal surface type and vegetation variability, can be made to the emissivity maps before these satellite data are available. A surface type can change from green vegetation to brown vegetation and then to bare soil over the course of a year. The current map will be modified to take seasonal variations into account. There are additional effects on surface emissivity that have yet to be considered; however, the current map is a first step in defining more accurate surface emissivities.

Accessing the emissivity maps

The broadband, CERES window and Fu-Liou band surface emissivity maps may be viewed and the data downloaded from the web site:

http://tanalo.larc.nasa.gov:8080/surf_htmls/SARB_surf.html

Sample pages from this web site are given in Appendix C..

Figure 7. Broadband Longwave Surface Emissivity, 2.5^{o} equal-area grid.

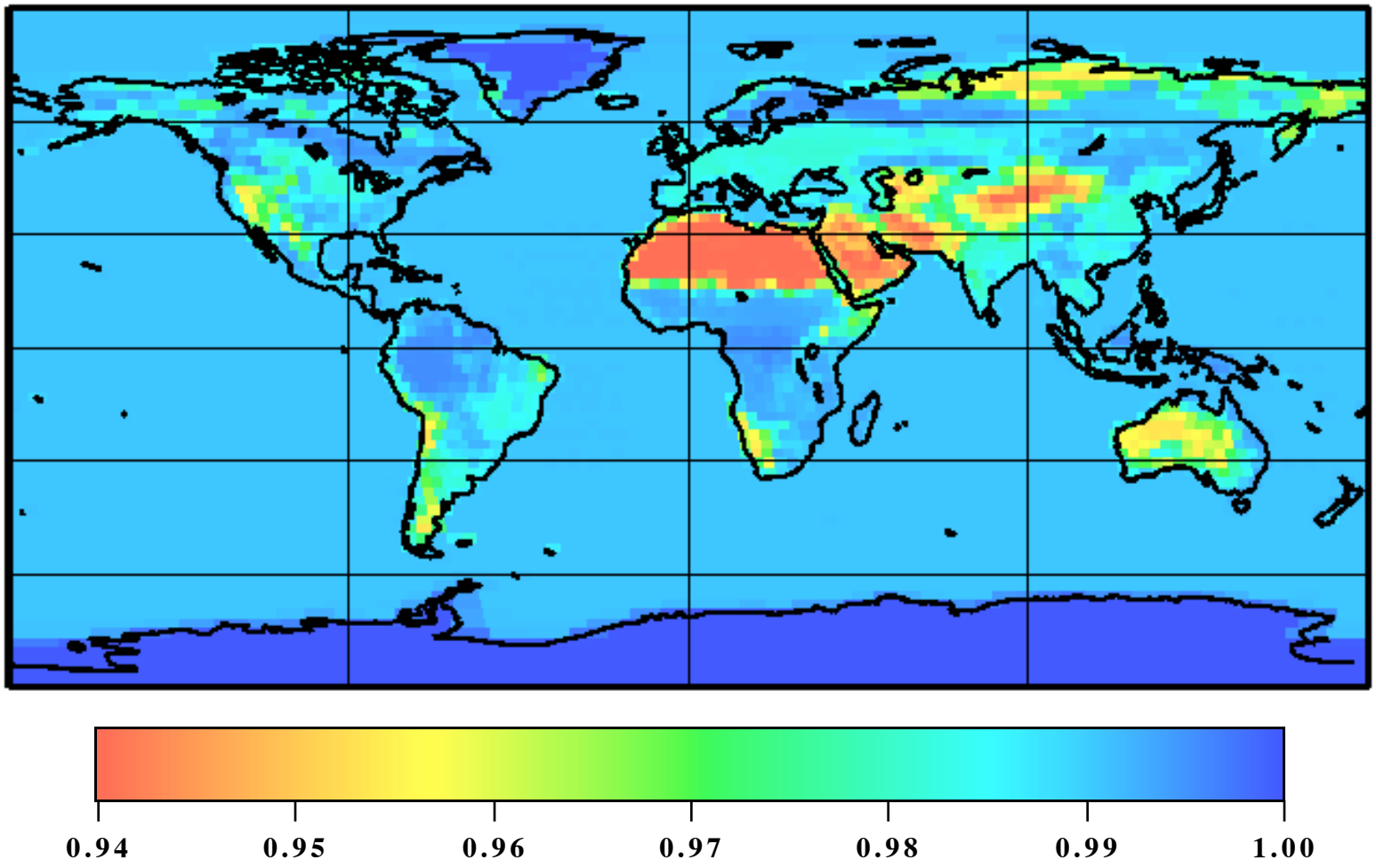

Figure 8. Surface Net Longwave Flux (Wm^{-2}) for October 1986.

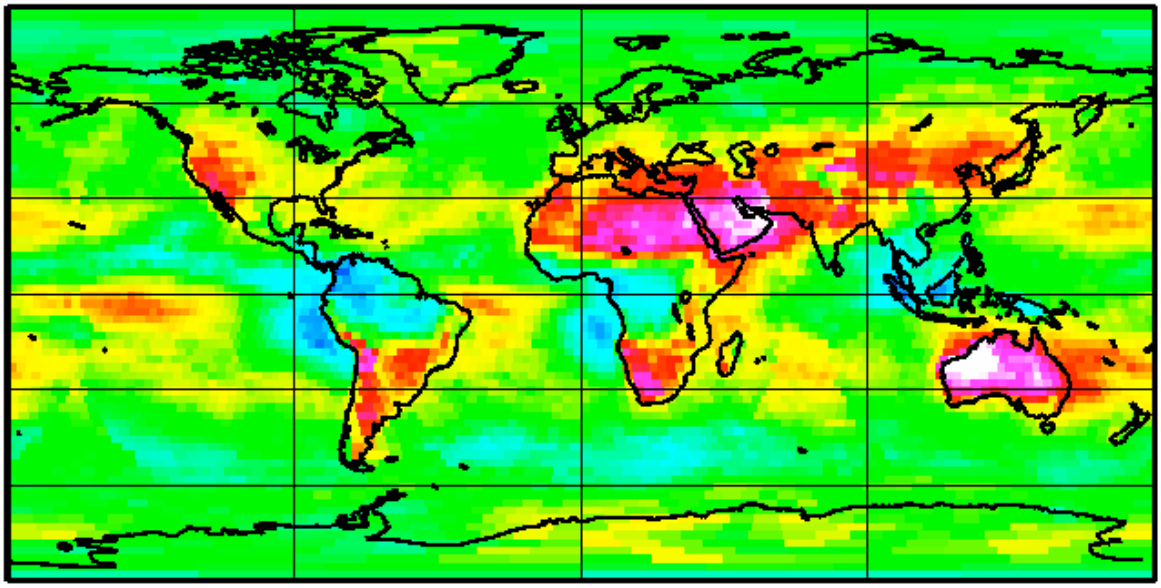

(a) Emissivity = 1

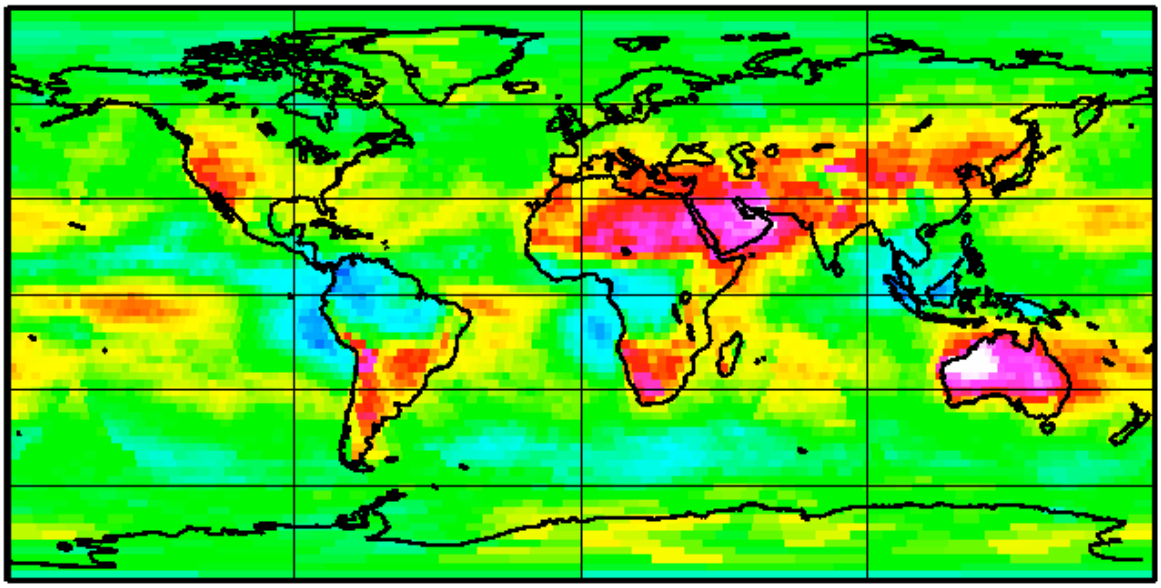

(b) Emissivity from map

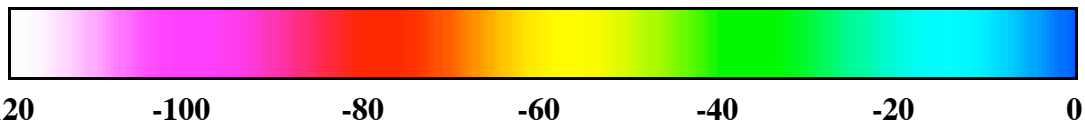

Figure 9: Difference in NLW Flux (Wm^{-2}) : Flux with variable variable ε - flux with constant ε

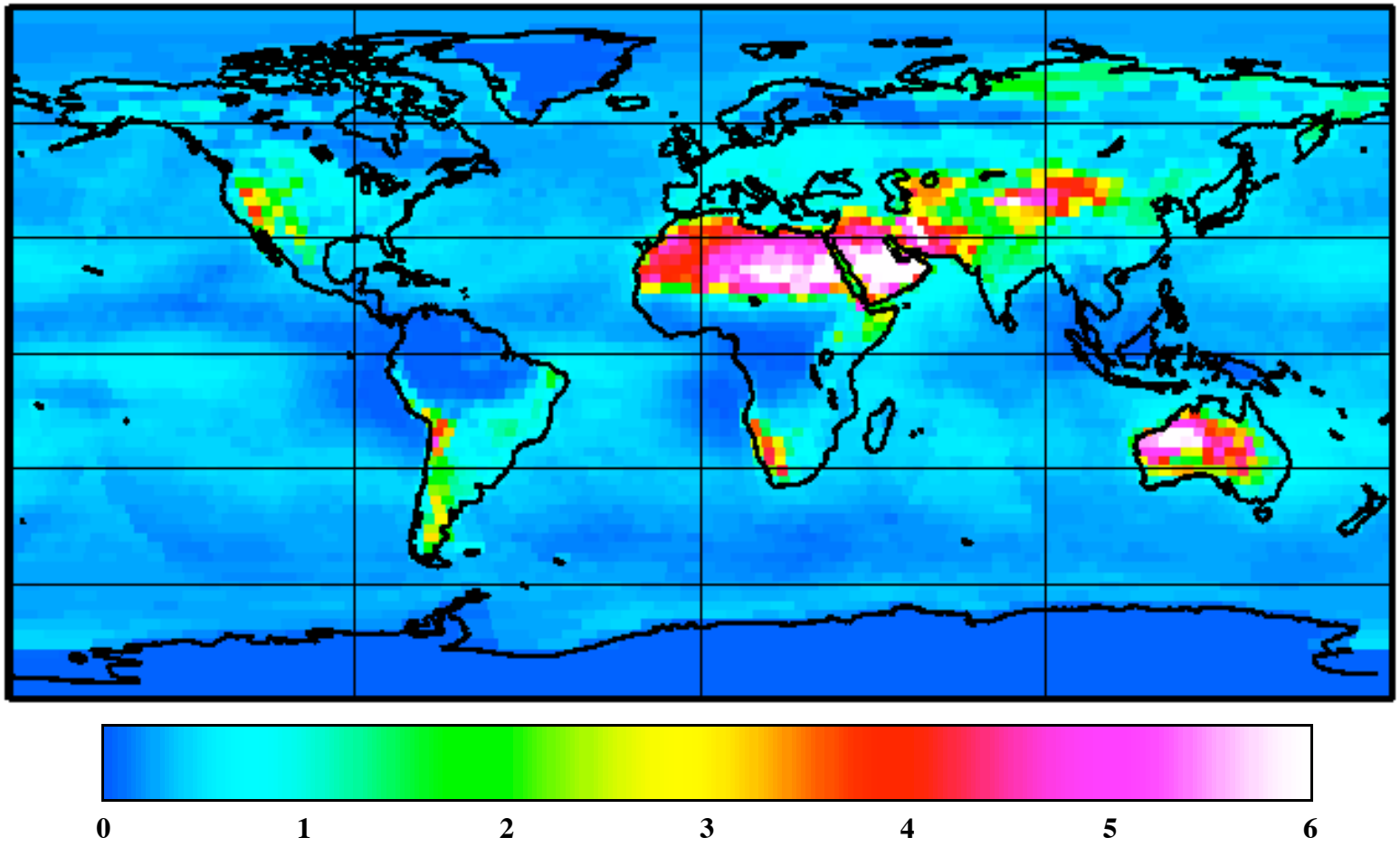

Appendix A.

The following description of IGBP surface types are adopted from Belward and Loveland (1996).

1. Evergreen Needleleaf Forests: Surface is dominated by trees with a canopy cover of over 60% and height exceeding 2 meters. Almost all trees remain green all year. Canopy is never without green foliage.

2. Evergreen Broadleaf Forests: Surface is dominated by trees with a canopy cover of over 60% and height exceeding 2 meters. Almost all trees remain green all year. Canopy is never without green foliage.

3. Deciduous Needleleaf Forests: Surface is dominated by trees with a canopy cover of over 60% and height exceeding 2 meters. Consists of seasonal needleleaf trees with an annual cycle of leaf-on and leaf-off periods.

4. Deciduous Broadleaf Forests: Surface is dominated by trees with a canopy cover of over 60% and height exceeding 2 meters. Consists of seasonal broadleaf trees with an annual cycle of leaf-on and leaf-off periods.

5. Mixed Forests: Surface is dominated by trees with a canopy cover of over 60% and height exceeding 2 meters. Consists of tree communities with interspersed mixtures or mosaics of the other four forest cover types. None of the forest types exceeds 60% of the landscape.

6. Closed Shrublands: Surface consists of woody vegetation less than 2 meters tall and with shrub canopy cover of over 60%. The shrub foliage can be either evergreen or deciduous.

7. Open Shrublands: Surface consists of woody vegetation less than 2 meters tall and with shrub canopy cover between 10–60%. The shrub foliage can be either evergreen or deciduous.

8. Woody Savannahs: Surface consists of herbaceous and other understory systems, and with forest canopy cover between 30–60%. The forest cover height exceeds 2 meters.

9. Savannahs: Surface consists of herbaceous and other understory systems, and with forest canopy cover between 10–30%. The forest cover height exceeds 2 meters.

10. Grasslands: Surface consists of herbaceous types of cover. Tree and shrub cover is less than 10%.

11. Permanent Wetlands: Surface consists of a permanent mixture of water and herbaceous or woody vegetation that cover extensive areas. The vegetation can be present in either salt, brackish, or fresh water.

12. Croplands: Surface is covered with temporary crops followed by harvest and a bare soil period (e.g., single and multiple cropping systems.) Note that perennial woody crops will be classified as the appropriate forest or shrub land cover type.

13. Urban and Built-Up: Surface is covered by buildings and other man-made structures. Note that this class will not be mapped from the AVHRR imagery but will be developed from the populated places layer that is part of the Digital Chart of the World (Danko, 1992).

14. Cropland/Natural Vegetation Mosaics: Surface consists of a mosaic of croplands, forest, shrublands, and grasslands in which no one component comprises more than 60% of the landscape.

15. Snow and Ice: Surface is under snow and/or ice cover throughout the year.

16. Barren: Surface is made up of exposed soil, sand, rocks, or snow which never have more than 10% vegetated cover during any time of the year.

17. Water Bodies: Oceans, seas, lakes, reservoirs, and rivers. The water bodies can be composed of either fresh or salt water.

18. Tundra: Surface is defined by IGBP to be Barren but is also identified by the Olson vegetation map (Olson et al. 1985), as tundra (Arctic wetlands).

More information on IGBP is available from the web sites: http://www.igbp.kva.se

and: http://www.ngdc.noaa.gov:80/paleo/igbp-dis/index.html

Appendix B.

Emissivity Values for the Fu-Liou Longwave Bands 1–7.

Surface Type	Fu-Liou 1	Fu-Liou 2	Fu-Liou 3	Fu-Liou 4	Fu-Liou 5	Fu-Liou 6	Fu-Liou 7
Evergreen Needleleaf	0.9891	0.9892	0.9900	0.9914	0.9908	0.9903	0.9898
Evergreen Broadleaf	0.9891	0.9892	0.9900	0.9914	0.9908	0.9903	0.9898
Deciduous Needleleaf	0.9849	0.9856	0.9841	0.9831	0.9789	0.9805	0.9733
Deciduous Broadleaf	0.9849	0.9856	0.9841	0.9831	0.9789	0.9805	0.9733
Mixed Forests	0.9870	0.9874	0.9870	0.9873	0.9848	0.9854	0.9815
Closed Shrublands	0.9490	0.9697	0.9738	0.9712	0.9474	0.9582	0.9663
Open Shrubland	0.8733	0.9340	0.9444	0.9390	0.8728	0.9038	0.9362
Woody Savannas	0.9867	0.9897	0.9920	0.9933	0.9830	0.9752	0.9853
Savannas	0.9867	0.9897	0.9920	0.9933	0.9830	0.9752	0.9853
Grasslands	0.9867	0.9897	0.9920	0.9933	0.9830	0.9752	0.9853
Permanent Wetlands	0.9828	0.9865	0.9870	0.9876	0.9832	0.9808	0.9870
Croplands	0.9867	0.9897	0.9920	0.9933	0.9830	0.9752	0.9853
Urban	1.0000	1.0000	1.0000	1.0000	1.0000	1.0000	1.0000
Mosaic	0.9868	0.9886	0.9895	0.9903	0.9839	0.9803	0.9834
Snow/Ice	0.9998	0.9998	0.9998	0.9998	0.9998	0.9999	0.9997
Barren	0.8353	0.9163	0.9342	0.9229	0.8354	0.8766	0.9210
Water	0.9788	0.9833	0.9819	0.9820	0.9835	0.9865	0.9886
Tundra	0.9469	0.9670	0.9883	0.9795	0.9751	0.9767	0.9920

Appendix B. (concluded)

Emissivity Values for the Fu-Liou Longwave Bands 8–12μm, the CERES Window Channel, and the Broadband.

Surface Type	Fu-Liou 8	Fu-Liou 9	Fu-Liou 10	Fu-Liou 11	Fu-Liou 12	CERES	Broadband
Evergreen Needleleaf	0.9948	1.0000	1.0000	1.0000	1.0000	0.9903	0.9956
Evergreen Broadleaf	0.9948	1.0000	1.0000	1.0000	1.0000	0.9903	0.9956
Deciduous Needleleaf	0.9869	1.0000	1.0000	1.0000	1.0000	0.9777	0.9900
Deciduous Broadleaf	0.9869	1.0000	1.0000	1.0000	1.0000	0.9777	0.9900
Mixed Forests	0.9908	1.0000	1.0000	1.0000	1.0000	0.9840	0.9928
Closed Shrublands	0.9747	0.9836	0.9836	0.9836	0.9836	0.9552	0.9837
Open Shrubland	0.9423	0.9509	0.9509	0.9509	0.9509	0.8974	0.9541
Woody Savannas	0.9928	1.0000	1.0000	1.0000	1.0000	0.9817	0.9932
Savannas	0.9928	1.0000	1.0000	1.0000	1.0000	0.9817	0.9932
Grasslands	0.9928	1.0000	1.0000	1.0000	1.0000	0.9817	0.9932
Permanent Wetlands	0.9824	0.9860	0.9860	0.9860	0.9860	0.9838	0.9920
Croplands	0.9928	1.0000	1.0000	1.0000	1.0000	0.9817	0.9813
Urban	1.0000	1.0000	1.0000	1.0000	1.0000	1.0000	1.0000
Mosaic	0.9918	1.0000	1.0000	1.0000	1.0000	0.9828	0.9830
Snow/Ice	0.9994	0.9995	0.9995	0.9995	0.9995	0.9998	0.9999
Barren	0.9262	0.9345	0.9345	0.9345	0.9345	0.8686	0.9412
Water	0.9719	0.9719	0.9719	0.9719	0.9719	0.9860	0.9907
Tundra	0.9888	0.9888	0.9888	0.9888	0.9888	0.9806	0.9918

Appendix C.

Sample pages from the web site:

http://tanalo.larc.nasa.gov:8080/surf_htmls/SARB_surf.html

For questions or problems involving the site, please contact :

d.a.rutan@larc.nasa.gov

Surface &
Atmospheric
Radiation
Budget

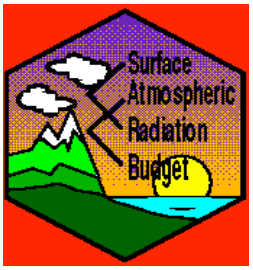

CERES *Surface Properties Home Page*

The SARB working group, part of the Clouds and the Earth's Radiant Energy System CERES mission, will calculate profiles of shortwave and longwave fluxes from the surface to the top of the atmosphere. The radiation transfer code which will be used was developed by Qiang Fu and Kuo Nan Liou, (Fu & Liou Model) For proper results the surface boundary condition must be specified as a function of the spectral bands of the model based upon the varying scenes that the instrument will be observing. For your perusal we've placed a set of images (Access Here) that contain the data which will be the starting points for these lower boundary conditions. For a more detailed description of how these surface maps are applied in the SARB processing consider reading the Surface Properties Description Page.

New Click here for NEWS and updates to these pages. (Latest update: 05/05/99)

Current Data

The various data available are listed in the button box below. The images of all but the snow and ice data are interactive so if you desire to see an area more closely, aim your pointer in the general area you would like to see in detail. If you are interested in a specific latitiude and longitude use the *Data by Lat/long* button to find out all of aour current surface information for that location.

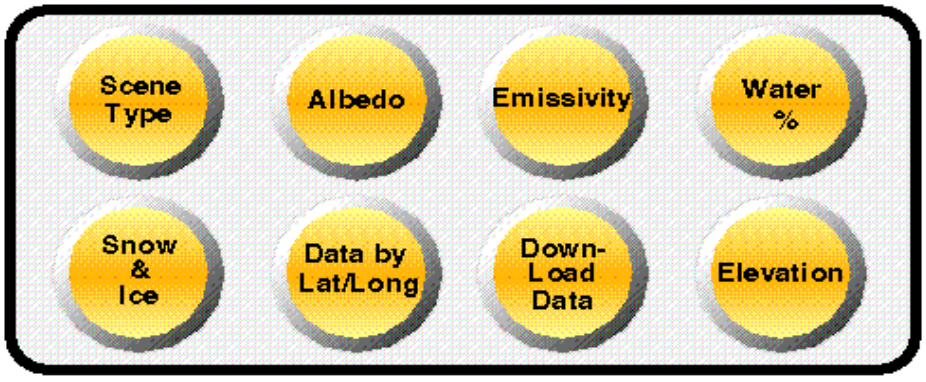

CERES/SARB Surface Maps for Download

This page lists all the available information for easy downloading of the maps. All maps, except the digital elevation map are 8-bit binary data made on a Sun SPARC Workstation. Their size is 2160 points in longitude, 1080 points in latitude or 1/6 degree equal angle. All maps begin at the North Pole, Greenwich Meridian. To download a map click on the "MAP" icon or the word "Download", using the right mouse button if you're using NETSCAPE.

- Netscape users, use "save link as" under the right mouse button.

Available CERES Surface Data

	Data Description	Range of Values	Related Link	Last Update
Download	IGBP+1 CERES scene type map (~2.3Mb)	1 to 18	Discussion	Dec. 03, 1998
Download	Map of Surface Albedo(*100) @ 60Deg Solar Zenith Angle. (~2.3Mb)	0 to 100	Discussion	Dec. 03, 1998
Download	Map of Broadband Surface Emissivity(*100).(~2.3Mb)	0 to 100	Discussion	Dec. 03, 1998
Download	Map of Window (8-12Micron) Surface Emissivity(*100).(~2.3Mb)	0 to 100	Discussion	Dec. 03, 1998
Download	Percentage of water in each 10' grid box.(~2.3Mb)	0 to 100	Discussion	Aug. 01, 1997
Download	Digital elevation in each 10' grid box. (Water bodies equal -9999.) (~4.6Mb)	-500 to 7000 (meters)	Discussion	Aug. 01, 1997
Download	Snow Map for October, 1986.(~2.3Mb)	0 to 150 (inches)	Discussion	Aug. 01, 1997
Download	Ice Map for October, 1986.(~2.3Mb)	0 to 100 (%)	Discussion	Aug. 01, 1997
Download	Data tables that create the maps.	-	Discussion	May 15, 1998
Download	Spectral emissivities in the 12 Longwavebands of the Fu & Liou code.	-	Discussion	May 15, 1998

Back to Surface Properties Home Page

References:

Belward, A. and T. Loveland, 1996: The DIS 1-km land cover data set. *GLOBAL CHANGE, The IGBP Newsletter*, **27**.

Caselles, V., E. Valor, C. Cesar, and E. Rubio, 1997: Thermal band selection for the PRISM instrument: 1. Analysis of emissivity-temperature separation algorithms. *Journal of Geophysical Research*, **102**, 11145–11164.

Danko, D. M., 1992: The digital chart of the world. *Geoinfosystems*, **2**, 29–36.

Fu, Q. and K. N. Liou, 1992: On the correlated *k*-distribution method for radiative transfer in nonhomogeneous atmospheres. *Journal of the Atmospheric Sciences*, **49**, 2139–2156.

Gupta, S. K., W. L. Darnell, and A. C. Wilber, 1992: A parameterization for longwave surface radiation from satellite data: Recent improvements. *Journal of Applied Meteorology*, **31**, 1361–1367.

Kahle, A. B. and R. E. Alley, 1992: Separation of temperature and emittance in remotely sensed radiance measurements. *Remote Sensing of the Environment*, **42**, 107–111.

Kealy, P. A. and S. J. Hook, 1993: Separating temperature and emissivity in thermal infrared multispectral scanner data: Implications for recovering land surface temperatures. *IEEE Transactions on Geoscience and Remote Sensing*, **31**, 1155–1164.

Kratz, D. P. and F. G. Rose, 1999: Accounting for molecular absorption within the spectral range of the CERES window channel. *Journal of Quantitative Spectroscopy and Radiative Transfer,* **61**, 83–95.

Liou, K. N., Q. Fu, and T. P. Ackerman, 1988: A simple formulation of the delta-four-stream approximation for radiative transfer parameterization. *Journal of the Atmospheric Sciences*, **45**, 1940–1947.

Masusda, K., T. Takashima, and Y. Takayama , 1988: Emissivity of pure and sea waters for the model sea surface in the infrared window regions. *Remote Sensing of the Environment*, **24**, 313–329.

Olioso, A., 1995: Simulating the relationship between thermal emissivity and Normalized Difference Vegetation Index. *International Journal of Remote Sensing*, **16**, 3211–3216.

Olson, J. S., J. A. Watts, and L.J. Allison, 1985: Major world ecosystem complexes ranked by carbon in live vegetation. NDP017, Carbon Dioxide Information Analysis Center, Oak Ridge National Laboratory, Oak Ridge, Tennessee.

Prabhakara, C., D. P. Kratz, J.-M. Yoo, G. Dalu, and A. Vernekar, 1993: Optically thin cirrus clouds: Radiative impact on the warmpool. *Journal of Quantitative Spectroscopy and Radiative Transfer*, **49**, 467–483.

Rees, W. G. , 1993: Infrared emissivities of Arctic land cover types. *International Journal of Remote Sensing*, **14**, 1013–1017.

Rutan, D. A. and T. P. Charlock, 1997: Spectral reflectance, directional reflectance, and broadband albedo of the Earth's surface. *Proceedings of the AMS Ninth Conference on Atmospheric Radiation, Long Beach, CA,* February 2–7, 466–470.

Salisbury, J. W. and D. M. D'Aria, 1992a: Emissivity of terrestrial materials in the 8–14 μm atmospheric

window. *Remote Sensing of the Environment*, **42**, 83–106.

Salisbury, J. W. and D. M. D'Aria, 1992b: Infrared (8–14 μm) remote sensing of soil particle size. *Remote Sensing of the Environment,* **42**, 157–165.

Smith, W. L., R. O. Knuteson, H. E. Revercomb, W. Feltz, H. B. Howell, W. P. Menzel, N. R. Nalli, O. Brown, J. Brown, P. Minnett, and W. McKeown, 1996: Observations of the infrared radiative properties of the ocean- Implications for the measurement of sea surface temperature via satellite remote sensing. *Bulletin of the American Meteorological Society*, **77**, 41–51.

Snyder, W. C., Z. Wan, Y. Zhang, and Y.-Z Feng, 1998: Classification-based emissivity for land surface temperature measurement from space. *International Journal of Remote Sensing*, **19,** 2753–2774.

Snyder, W. C. and Z. Wan, 1996: Surface temperature correction for active infrared reflectance measurements of natural materials. *Applied Optics*, **35**, 2216–2220.

Snyder, W. C., Z. Wan, Y. Ahang and Y. -Z. Feng, 1997: Thermal infrared (3–14 μm) bidirectional reflectance measurements of sands and soils. *Remote Sensing of the Environment*, **60**, 101–109.

Van de Griend, A. A. and M. Owe, 1993: On the relationship between thermal emissivity and Normalized Vegetation Index for natural surfaces. *International Journal of Remote Sensing*, **14**, 1119–1131.

Wan, Z. and J. Dozier, 1996: A generalized split-window algorithm for retrieving land-surface temperature from space. *IEEE Transactions on Geoscience and Remote Sensing*, **34**, 892–905.

Wielicki, B. A., B. R. Barkstrom, E. F. Harrison, R. B. Lee III, G. L. Smith, and J. E. Cooper, 1996: Clouds and the Earth's Radiant Energy System (CERES): An Earth Observing System experiment, *Bulletin of the American Meteorological Society*, **77**, 853–868.

Wu, X. and W. L. Smith, 1997: Emissivity of rough sea surface for 8–13 μm: Modeling and verification. *Applied Optics*, **36**, 2609–2619.

Zobler, L., 1986: A world soil file for global climate modeling. NASA TM 87802, 35 pp.

REPORT DOCUMENTATION PAGE

Form Approved
OMB No. 0704-0188

1. AGENCY USE ONLY (Leave blank)	2. REPORT DATE	3. REPORT TYPE AND DATES COVERED
	August 1999	Technical Publication

4. TITLE AND SUBTITLE
Surface Emissivity Maps for Use in Satellite Retrievals of Longwave Radiation

5. FUNDING NUMBERS
291-01-60-00

6. AUTHOR(S)
Anne C. Wilber, David P. Kratz, and Shashi K. Gupta

7. PERFORMING ORGANIZATION NAME(S) AND ADDRESS(ES)
NASA Langley Research Center
Hampton, VA 23681-2199

8. PERFORMING ORGANIZATION REPORT NUMBER
L-17861

9. SPONSORING/MONITORING AGENCY NAME(S) AND ADDRESS(ES)
National Aeronautics and Space Administration
Washington, DC 20546-0001

10. SPONSORING/MONITORING AGENCY REPORT NUMBER
NASA/TP-1999-209362

11. SUPPLEMENTARY NOTES
A.C. Wilber and S. K. Gupta - Analytical Services and Materials, Inc., Hampton, VA
D. P. Kratz - NASA Langley Research Center, Hampton

12a. DISTRIBUTION/AVAILABILITY STATEMENT
Unclassified-Unlimited
Subject Category 47 Distribution: Standard
Availability: NASA CASI (301) 621-0390

12b. DISTRIBUTION CODE

13. ABSTRACT (Maximum 200 words)
Accurate accounting of surface emissivity is essential for the retrievals of surface temperature from remote sensing measurements, and for the computations of longwave (LW) radiation budget of the Earth's surface. Past studies of the above topics assumed that emissivity for all surface types, and across the entire LW spectrum is equal to unity. There is strong evidence, however, that emissivity of many surface materials is significantly lower than unity, and varies considerably across the LW spectrum. We have developed global maps of surface emissivity for the broadband LW region, the thermal infrared window region (8-12 micron), and 12 narrow LW spectral bands. The 17 surface types defined by the International Geosphere Biosphere Programme (IGBP) were adopted as such, and an additional (18th) surface type was introduced to represent tundra-like surfaces. Laboratory measurements of spectral reflectances of 10 different surface materials were converted to corresponding emissivities. The 10 surface materials were then associated with 18 surface types. Emissivities for the 18 surface types were first computed for each of the 12 narrow spectral bands. Emissivities for the broadband and the window region were then constituted from the spectral band values by weighting them with Planck function energy distribution

14. SUBJECT TERMS
Surface Emissivity, Surface Materials, Longwave Radiation
Surface Temperatures, Climate Models, CERES

15. NUMBER OF PAGES
35

16. PRICE CODE
A03

17. SECURITY CLASSIFICATION OF REPORT	18. SECURITY CLASSIFICATION OF THIS PAGE	19. SECURITY CLASSIFICATION OF ABSTRACT	20. LIMITATION OF ABSTRACT
Unclassified	Unclassified	Unclassified	UL